Constraining M_ν with the Bispectrum II: the Total Information Content of the Galaxy Bispectrum

ChangHoon Hahn,[1, 2, 3, *] Francisco Villaescusa-Navarro,[3, 4] and ...

[1]*Lawrence Berkeley National Laboratory, 1 Cyclotron Rd, Berkeley CA 94720, USA*
[2]*Berkeley Center for Cosmological Physics, University of California, Berkeley, CA 94720, USA*
[3]*Department of Astrophysical Sciences, Princeton University, Peyton Hall, Princeton NJ 08544, USA*
[4]*Center for Computational Astrophysics, Flatiron Institute, 162 5th Avenue, New York, NY 10010, USA*

(Dated: `DRAFT --- 53b06db --- 2020-10-19 --- NOT READY FOR DISTRIBUTION`)

ABSTRACT

Massive neutrinos suppress the growth of structure on small scales and leave an imprint on large-scale structure that can be measured to constrain their total mass, M_ν. With standard analyses of two-point clustering statistics, M_ν constraints are severely limited by parameter degeneracies. Hahn et al. (2020) demonstrated that the bispectrum, the next higher-order statistic, can break these degeneracies and dramatically improve constraints on M_ν and other cosmological parameters. In this paper, we present the constraining power of the *redshift-space galaxy bispectrum*, B_0^g. We construct the Molino suite: $75,000$ mock galaxy catalogs constructed from the Quijote N-body simulations using the halo occupation distribution (HOD) model, which provides an effective galaxy bias framework well-suited for simulation-based approaches. Using these mocks, we present Fisher matrix forecasts for $\{\Omega_{\rm m}, \Omega_{\rm b}, h, n_s, \sigma_8, M_\nu\}$ and quantify, for the first time, the total information content of the B_0^g down to nonlinear scales. For $k_{\rm max}=0.5\,h/{\rm Mpc}$, B_0^g improves constraints on $\Omega_{\rm m}$, $\Omega_{\rm b}$, h, n_s, and σ_8 by 2.8, 3.1, 3.8, 4.2, 4.2, and 4.7× over power spectrum, after marginalizing over HOD parameters. For M_ν, we achieve 5.6× tighter constraints with B_0^g. Even with priors from *Planck*, B_0^g improves all of the cosmological constraints by $\gtrsim$ 2×. While effects such as survey geometry and assembly bias will have an impact, these constraints are derived for $(1\ h^{-1}{\rm Gpc})^3$, a substantially smaller volume than upcoming surveys. Therefore, we conclude that including the galaxy bispectrum will significantly improve cosmological constraints for upcoming galaxy surveys — especially for M_ν.

Keywords: cosmology: cosmological parameters — cosmology: large-scale structure of Universe. — cosmology: theory

* hahn.changhoon@gmail.com

1. INTRODUCTION

More than two decades ago, neutrino oscillation experiments discovered the lower bound on the sum of neutrino masses ($M_\nu \gtrsim 0.06$ eV) and confirmed physics beyond the Standard Model (Fukuda et al. 1998; Forero et al. 2014; Gonzalez-Garcia et al. 2016). Since then, experiments have sought to measure M_ν more precisely in order to distinguish between the 'normal' and 'inverted' neutrino mass hierarchy scenarios and further reveal the physics of neutrinos. Upcoming laboratory experiments (*e.g.* double beta decay and tritium beta decay), however, will *not* place the most stringent constraints on M_ν (Bonn et al. 2011; Drexlin et al. 2013). Complementary and more precise constraints on M_ν can be placed by measuring the effect of neutrinos on the expansion history and growth of cosmic structure.

In the early Universe, neutrinos are relativistic and contribute to the energy density of radiation. Later, as they become non-relativistic, they contribute to the energy density of matter. This transition affects the expansion history of the Universe and leaves imprints on the cosmic microwave background (CMB; Lesgourgues & Pastor 2012, 2014). Massive neutrinos also impact the growth of structure. While neutrino perturbations are indistinguishable from cold dark matter (CDM) perturbations on large scales, below their free-streaming scale, neutrinos do not contribute to the clustering and reduce the amplitude of the total matter power spectrum. They also reduce the growth rate of CDM perturbations on small scales. This combined suppression of the small-scale matter power spectrum leaves measurable imprints on the CMB as well as large-scale structure (for further details see Lesgourgues & Pastor 2012, 2014; Gerbino 2018).

The tightest cosmological constraints on M_ν currently come from combining CMB temperature and large-angle polarization data from the *Planck* satellite with Baryon Acoustic Oscillation and CMB lensing: $M_\nu < 0.13$ eV (Planck Collaboration et al. 2018). Future improvements will likely continue to come from combining CMB data on large scales with clustering/lensing data on small scales and low redshifts, where the suppression of power by neutrinos is strongest (Brinckmann et al. 2019). But they will heavily rely on a better determination of τ, the optical depth of reionization since CMB experiments measure the combined quantity $A_s e^{-2\tau}$ (Allison et al. 2015; Liu et al. 2016; Archidiacono et al. 2017). Major upcoming CMB experiments, however, are ground-based (*e.g.* CMB-S4) and will not directly constrain τ (Abazajian et al. 2016). Meanwhile, proposed future space-based experiments such as LiteBIRD[1] and LiteCOrE[2], which have the greatest potential to precisely measure τ, have yet to be confirmed.

Despite the τ bottleneck in the near future, measuring the M_ν imprint on the 3D clustering of galaxies provides a promising avenue for improving M_ν constraints. Upcoming galaxy surveys such as DESI[3], PFS[4], EUCLID[5], and the Roman Space Telescope[6], with the unprecedented cosmic volumes they will probe, have the potential to tightly constrain M_ν (Audren et al. 2013; Font-Ribera et al. 2014; Petracca et al. 2016; Sartoris et al. 2016; Boyle & Komatsu 2018). Constraining M_ν

---

[1] http://litebird.jp/eng/
[2] http://www.core-mission.org/
[3] https://www.desi.lbl.gov/
[4] https://pfs.ipmu.jp/
[5] http://sci.esa.int/euclid/
[6] https://roman.gsfc.nasa.gov/

from 3D galaxy clustering, however, faces two major challenges: (1) accurate theoretical modeling beyond linear scales, for bias tracers in redshift-space and (2) parameter degeneracies that limit the constraining power of standard two-point clustering analyses.

For the former, simulations have made huge strides in accurately modeling nonlinear structure formation with massive neutrinos (*e.g.* Brandbyge et al. 2008; Villaescusa-Navarro et al. 2013; Castorina et al. 2015; Adamek et al. 2017; Emberson et al. 2017; Banerjee et al. 2018; Villaescusa-Navarro et al. 2018, 2019; Yoshikawa et al. 2020). Moreover, new simulation-based approaches to modeling such as 'emulation' enable us to tractably exploit the accuracy of N-body simulations and analyze galaxy clustering on nonlinear scales beyond traditional perturbation theory methods. Recent works have applied these simulation-based approaches to analyze small-scale galaxy clustering with remarkable success (*e.g.* Heitmann et al. 2009; Kwan et al. 2015; Euclid Collaboration et al. 2018; Lange et al. 2019; Zhai et al. 2019; Wibking et al. 2019). These developments present the opportunity to significantly improve M_ν constraints by unlocking the information content in nonlinear clustering, where the impact of massive neutrinos is strongest (*e.g.* Brandbyge et al. 2008; Saito et al. 2008; Wong 2008; Saito et al. 2009; Viel et al. 2010; Agarwal & Feldman 2011; Marulli et al. 2011; Bird et al. 2012; Castorina et al. 2015; Banerjee & Dalal 2016; Upadhye et al. 2016; Banerjee & Abel 2020; Allys et al. 2020; Massara et al. 2020; Uhlemann et al. 2020).

For the latter, parameter degeneracies such as the M_ν–σ_8 degeneracy pose serious limitations on constraining M_ν with the power spectrum (Villaescusa-Navarro et al. 2018). However, information in the nonlinear regime cascades from the power spectrum to higher-order statistics such as the bispectrum and help break these degeneracies (Hahn et al. 2020). Previous studies have already demonstrated the potential of the bispectrum for improving cosmological parameter constraints (Sefusatti & Scoccimarro 2005; Sefusatti et al. 2006; Chan & Blot 2017; Yankelevich & Porciani 2019; Agarwal et al. 2020). Chudaykin & Ivanov (2019), in particular, included M_ν in their forecast and found that the bispectrum significantly improves constraints on M_ν. However, none of these perturbation theory based forecast includes the constraining power on nonlinear scales.

In Hahn et al. (2020), the previous paper of this series, we used 22,000 N-body simulations from the Quijote suite to quantify the total information content and constraining power of the redshift-space halo bispectrum down to nonlinear scales. For $k_{\rm max}$=0.5 h/Mpc, we found that the bispectrum achieves $\Omega_{\rm m}$, $\Omega_{\rm b}$, h, n_s, and σ_8 constraints 1.9, 2.6, 3.1, 3.6, and 2.6 times tighter than the power spectrum. For M_ν, the bispectrum improved constraints by 5 times over the power spectrum. In this forecast, we marginalized over linear bias, b_1, and halo mass limit, $M_{\rm lim}$, parameters. We also found that the improvements from the bispectrum are not impacted when we include quadratic and nonlocal bias parameters in the forecast. Nevertheless, Hahn et al. (2020) focused on the halo bispectrum. Actual constraints on M_ν, however, will be derived from the distribution of galaxies and therefore require a more realistic and complete galaxy bias model, which we provide in this paper.

In this work, we present the total information content and constraining power of the *redshift-space galaxy bispectrum* down to $k_{\rm max} = 0.5$ h/Mpc. For our galaxy bias model, we use the halo occupation distribution (HOD) framework, which provides a statistical prescription for populating dark matter halos with central and satellite galaxies. The HOD model has been successful in reproducing the

Table 1. The QUIJOTE suite includes 15,000 N-body simulations at the fiducial cosmology to accurately estimate the covariance matrices. It also includes sets of 500 simulations at 14 other cosmologies, where only one parameter is varied from the fiducial value (underlined), to estimate derivatives of observables along the cosmological parameters.

Name	M_ν	Ω_m	Ω_b	h	n_s	σ_8	ICs	realizations
Fiducial	0.0	0.3175	0.049	0.6711	0.9624	0.834	2LPT	15,000
Fiducial ZA	0.0	0.3175	0.049	0.6711	0.9624	0.834	Zel'dovich	500
M_ν^+	0.1 eV	0.3175	0.049	0.6711	0.9624	0.834	Zel'dovich	500
M_ν^{++}	0.2 eV	0.3175	0.049	0.6711	0.9624	0.834	Zel'dovich	500
M_ν^{+++}	0.4 eV	0.3175	0.049	0.6711	0.9624	0.834	Zel'dovich	500
Ω_m^+	0.0	0.3275	0.049	0.6711	0.9624	0.834	2LPT	500
Ω_m^-	0.0	0.3075	0.049	0.6711	0.9624	0.834	2LPT	500
Ω_b^+	0.0	0.3175	0.051	0.6711	0.9624	0.834	2LPT	500
Ω_b^-	0.0	0.3175	0.047	0.6711	0.9624	0.834	2LPT	500
h^+	0.0	0.3175	0.049	0.6911	0.9624	0.834	2LPT	500
h^-	0.0	0.3175	0.049	0.6511	0.9624	0.834	2LPT	500
n_s^+	0.0	0.3175	0.049	0.6711	0.9824	0.834	2LPT	500
n_s^-	0.0	0.3175	0.049	0.6711	0.9424	0.834	2LPT	500
σ_8^+	0.0	0.3175	0.049	0.6711	0.9624	0.849	2LPT	500
σ_8^-	0.0	0.3175	0.049	0.6711	0.9624	0.819	2LPT	500

observed galaxy clustering (*e.g.* Zheng et al. 2005; Leauthaud et al. 2012; Tinker et al. 2013; Zentner et al. 2016; Vakili & Hahn 2019). It is also the primary framework used in simulation-based clustering analyses (*e.g.* McClintock et al. 2018; Zhai et al. 2019; Lange et al. 2019; Wibking et al. 2019). We first construct 75,000 galaxy mock catalogs from the QUIJOTE N-body simulations then use them to calculate Fisher matrix forecasts. Afterward, we present the constraining power of the galaxy bispectrum on M_ν and other cosmological parameters after marginalizing over the HOD parameters. This work is the second paper in a series that aims to demonstrate the potential for simulation-based galaxy bispectrum analyses in constraining M_ν. Later in the series, we will also present methods to tackle challenges that come with analyzing the full galaxy bispectrum, such as data compression to reduce its dimensionality. The series will culminate in a fully simulation-based $P_0^g + P_2^g$ and B_0^g reanalysis of SDSS-III BOSS.

In Sections 2 and 3, we describe the QUIJOTE N-body simulation suite and the HOD framework we use to construct the MOLINO suite of galaxy mock catalogs from them. We then describe in Section 4, how we measure the bispectrum and calculate the Fisher forecasts of the cosmological parameters from the galaxy mocks. Finally, in Section 5, we present the full information content of the galaxy bispectrum and demonstrate how it significantly improves the constraints on the cosmological parameters: Ω_m, Ω_b, h, n_s, σ_8, and *especially M_ν*.

2. THE QUIJOTE SIMULATION SUITE

For our forecasts we use simulations from the QUIJOTE suite, a set of over 43,000 N-body simulations that spans over 7,000 cosmological models and contains, at a single redshift, over 8.5 trillion particles (Villaescusa-Navarro et al. 2019). QUIJOTE was designed to quantify the information content of cosmological observables and train machine learning algorithms. It includes enough realizations to accurately estimate covariance matrices of high-dimensional observables, such as the bispectrum, as well as their derivatives with respect to cosmological parameters. For the derivatives, QUIJOTE includes sets of simulations run at different cosmologies where only one parameter is varied from the fiducial cosmology: Ω_m=0.3175, Ω_b=0.049, h=0.6711, n_s=0.9624, σ_8=0.834, and M_ν=0.0 eV. Along each $\theta \in \{\Omega_m, \Omega_b, h, n_s, \sigma_8\}$, the fiducial cosmology is adjusted by either a step above or below the fiducial value: θ^+ and θ^-. Along M_ν, because $M_\nu \geq 0.0$ eV and the derivative of certain observable with respect to M_ν is noisy, QUIJOTE includes sets of simulations for $\{M_\nu^+, M_\nu^{++}, M_\nu^{+++}\} = \{0.1, 0.2, 0.4$ eV$\}$. See Table 1 for a summary of the QUIJOTE simulations used in this work.

The initial conditions for all the simulations were generated at z=127 using second-order perturbation theory for simulations with massless neutrinos ($M_\nu = 0.0$ eV) and the Zel'dovich approximation for massive neutrinos ($M_\nu > 0.0$ eV). The initial conditions with massive neutrinos take their scale-dependent growth factors/rates into account using the Zennaro et al. (2017) method, while for the massless neutrino case we use the traditional scale-independent rescaling. From the initial conditions, the simulations follow the gravitational evolution of 512^3 dark matter particles, and 512^3 neutrino particles for $M_\nu > 0$ models, to $z = 0$ using GADGET-III TreePM+SPH code (Springel 2005). Simulations with massive neutrinos are run using the "particle method", where neutrinos are described as a collisionless and pressureless fluid and therefore modeled as particles, same as CDM (Brandbyge et al. 2008; ?). Halos are identified using the Friends-of-Friends algorithm (FoF; Davis et al. 1985) with linking length $b = 0.2$ on the CDM+baryon distribution. We refer readers to Villaescusa-Navarro et al. (2019) and Hahn et al. (2020) for further details on QUIJOTE. The QUIJOTE simulations are publicly available at https://github.com/franciscovillaescusa/Quijote-simulations.

3. HALO OCCUPATION DISTRIBUTION: THE MOLINO MOCK GALAXY CATALOGS

We are interested in quantifying the information content of the galaxy bispectrum. For a perturbation theory approach, this involves incorporating an analytic bias model for galaxies (*e.g.* Sefusatti et al. 2006; Yankelevich & Porciani 2019; Chudaykin & Ivanov 2019). Perturbation theory approaches, however, break down on small scales and cannot exploit the constraining power from the nonlinear regime. Instead, in our simulation-based approach, we use the halo occupation distribution (HOD) framework (*e.g.* Benson et al. 2000; Peacock & Smith 2000; Seljak 2000; Berlind & Weinberg 2002; Cooray & Sheth 2002; Zheng et al. 2005; Leauthaud et al. 2012; Tinker et al. 2013; Zentner et al. 2016; Vakili & Hahn 2019). HOD models statistically populate galaxies in dark matter halos by specifying the probability of a given halo hosting a certain number of galaxies. This statistical prescription for connecting galaxies to halos has been remarkably successful in reproducing the observed galaxy clustering and, as a result, is the standard approach for constructing simulated galaxy mock catalogs in
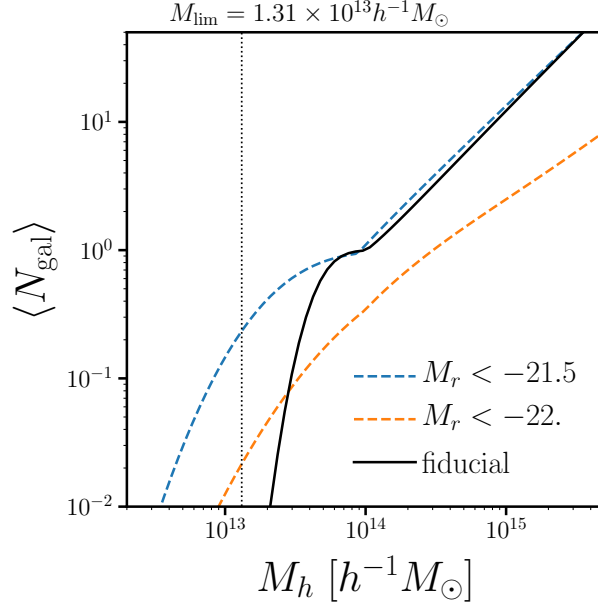
$$M_{\rm lim} = 1.31 \times 10^{13} h^{-1} M_\odot$$

Figure 1. Our fiducial halo occupation (black) parameterized using the standard Zheng et al. (2007) HOD model. The parameter values of our fiducial HOD model (Eq. 4) are roughly based on by the best-fit HOD parameters of the SDSS $M_r < -21.5$ and $< -22.$ samples from Zheng et al. (2007), modified to accommodate the $M_{\rm lim}=1.31\times10^{13}h^{-1}M_\odot$ halo mass limit of the QUIJOTE simulations (black dotted). We include the best-fit halo occupations of the SDSS $M_r < -21.5$ (blue dashed) and $< -22.$ samples (orange dashed) from Zheng et al. (2007) for reference. Since our HOD parameters are based on the high luminosity SDSS samples, we do not include assembly bias. Our fiducial HOD galaxy catalog has a galaxy number density of $\overline{n}_g \sim 1.63 \times 10^{-4} \ h^3/{\rm Mpc}^3$ and linear bias of $b_g \sim 2.55$.

galaxy clustering analyses to estimate covariance matrices and test systematic effects (*e.g.* Rodríguez-Torres et al. 2016, 2017; Beutler et al. 2017). More importantly, HOD is the primary framework used in simulation-based galaxy clustering analyses: *e.g.* emulation (McClintock et al. 2018; Zhai et al. 2019) or evidence modeling (Lange et al. 2019). Since the forecasts we present in this paper are aimed at quantifying the constraining power of the galaxy bispectrum for simulation-based analyses, the HOD model is particularly well-suited for our purpose.

In HOD models, the probability of a given halo hosting N galaxies of a certain class is dictated by its halo mass — $P(N|M_h)$. We use the standard HOD model from Zheng et al. (2007), which specifies the mean number of galaxies in a halo as

$$\langle N_{\rm gal}\rangle = \langle N_{\rm cen}\rangle + \langle N_{\rm sat}\rangle \tag{1}$$

with mean central galaxy occupation

$$\langle N_{\rm cen}\rangle = \frac{1}{2}\left[1 + {\rm erf}\left(\frac{\log M_h - \log M_{\rm min}}{\sigma_{\log M}}\right)\right] \tag{2}$$

and mean satellite galaxy occupation

$$\langle N_{\rm sat}\rangle = \langle N_{\rm cen}\rangle \left(\frac{M_h - M_0}{M_1}\right)^\alpha. \tag{3}$$

The mean number of centrals in a halo transitions smoothly from 0 to 1 for halos with mass $M_h > M_{min}$. The width of the transition is dictated by $\sigma_{\log M}$, which reflects the scatter between stellar mass/luminosity and halo mass. For $M_h > M_{min}$, $\langle N_{sat} \rangle$ follows a power law with slope α. M_0 is the halo mass cut-off for satellite occupation and $M_h = M_0 + M_1$ is the typical mass scale for halos to host one satellite galaxy. The numbers of centrals and satellites for each halo are drawn from Bernoulli and Poisson distribution, respectively. Central galaxies are placed at the center of the halo while the position and velocity of the satellite galaxies are sampled from a Navarro et al. (1997) (NFW) profile.

For the fiducial parameters of our HOD model, we use the following values:

$$\{\log M_{min}, \sigma_{\log M}, \log M_0, \alpha, \log M_1\} = \{13.65, \ 0.2, \ 14.0, \ 1.1, \ 14.0\}. \tag{4}$$

These values are roughly based on the best-fit HOD parameters for the SDSS $M_r < -21.5$ and -22 samples from Zheng et al. (2007). In Figure 1, we present the halo occupation of our fiducial HOD parameters (black). We include the best-fit halo occupations of the SDSS $M_r < -21.5$ (blue) and -22 (orange) samples from Zheng et al. (2007) for comparison. We also mark the $M_{lim} = 3.2 \times 10^{13} h^{-1} M_\odot$ halo mass limit of the QUIJOTE simulations (black dotted). At $M_h \sim 10^{13} M_\odot$, the best-fit halo occupations of the SDSS samples extend below M_{lim}. We, therefore, cannot use the exact best-fit HOD parameter values from the literature and instead reduce $\sigma_{\log M}$ to 0.2 dex. The high $\sigma_{\log M}$ in the $M_r < -21.5$ and -22 SDSS samples is caused by the turnover in the stellar-to-halo mass relation at high stellar masses (Mandelbaum et al. 2006; Conroy et al. 2007; More et al. 2011; Leauthaud et al. 2012; Tinker et al. 2013; Zu & Mandelbaum 2015; Hahn et al. 2019). Our fiducial halo occupation, with its lower $\sigma_{\log M}$, reflects a galaxy sample with a tighter scatter between stellar mass/luminosity and M_h than the SDSS samples. In practice, constructing such a sample would require selecting galaxies based on observable properties that correlate more strongly with M_h than luminosity or M_*. While there is evidence that such observables are available (*e.g.* L_{sat}; Alpaslan & Tinker 2019), they have not been adopted for selecting galaxy samples. Regardless, in this work our focus is on quantifying the information content of the galaxy bispectrum and not on analyzing a specific observed galaxy sample. We, therefore, opt for a more conservative set of HOD parameters with respect to M_{lim}, even if the resulting galaxy sample is less reflective of observations. For our fiducial halo occupation at the fiducial cosmology, the galaxy catalog has $\bar{n}_g \sim 1.63 \times 10^{-4} \ h^3 \ \text{Gpc}^{-3}$ and linear bias of $b_g \sim 2.55$.

The halo occupation in the Zheng et al. (2007) model depends solely on M_h. Simulations, however, find evidence that secondary halo properties such as concentration or formation history correlate with the spatial distribution of halos — a phenomenon referred to as "halo assembly bias" (*e.g.* Sheth & Tormen 2004; Gao et al. 2005; Harker et al. 2006; Wechsler et al. 2006; Dalal et al. 2008; **?**; Lacerna et al. 2014; Contreras et al. 2020; Hadzhiyska et al. 2020). A model that only depends on M_h, does not account for this halo assembly bias and may not be sufficiently flexible in describing the connection between galaxies and halos. Moreover, if unaccounted for in the HOD model, and thus not marginalized over, halo assembly bias can impact the cosmological parameter constraints. However, for the high luminosity SDSS samples ($M_r < -21.5$ and < -21), Zentner et al. (2016)

and Vakili & Hahn (2019) find little evidence for assembly bias in the galaxy clustering. Similarly, Beltz-Mohrmann et al. (2020) also find that the Zheng et al. (2007) HOD model is sufficient to reproduce galaxy clustering of luminous galaxies in hydrodynamic simulations. Since we base our HOD parameters on the high luminosity SDSS samples, we do not include assembly bias and use the Zheng et al. (2007) model.

The MOLINO suite of galaxy mock catalogs used in this paper are constructed using the 22,000 N-body simulations of the QUIJOTE suite: 15,000 at the fiducial cosmology and 500 at the 14 other cosmologies listed in Table 1. First, we construct mocks for estimating the covariance matrices using the 15,000 QUIJOTE simulations at the fiducial cosmology with the fiducial HOD parameters. Next, we construct mocks for estimating the derivatives with respect to cosmological parameters using the 500 QUIJOTE simulations at each of the 14 non-fiducial cosmologies. Finally, we construct mocks for estimating the derivatives with respect to the HOD parameters, using 500 QUIJOTE simulations at the fiducial cosmology with 10 sets of non-fiducial HOD parameters — a pair per parameter. Similar to the non-fiducial cosmologies in QUIJOTE, for each pair we vary one HOD parameter above and below the fiducial value by step sizes:

$$\{\Delta \log M_{\min}, \Delta \sigma_{\log M}, \Delta \log M_0, \Delta \alpha, \Delta \log M_1\} = \{0.05, 0.2, 0.2, 0.2, 0.2\}. \tag{5}$$

These step sizes were chosen so that the derivatives are converged. For the covariance matrix mocks, we generate one set of HOD realizations and apply RSD along the z-axis: 15,000 mocks. For the derivative mocks, we generate 5 sets of HOD realizations with different random seeds: 60,000 mocks. *In total, we construct and use 75,000 galaxy catalogs in our analysis.* The MOLINO galaxy catalogs are publicly available at where to access the galaxy catalogs.

TODO

4. BISPECTRUM AND COSMOLOGICAL PARAMETER FORECASTS

We measure the galaxy bispectrum and calculate the parameter constraints using the same methods as Hahn et al. (2020). For further details, we refer readers to Hahn et al. (2020).

To measure B_0^g, we use a Fast Fourier Transform (FFT) based estimator similar to the ones in Sefusatti & Scoccimarro (2005), Scoccimarro (2015), and Sefusatti et al. (2016). Galaxy positions are first interpolated onto a grid, $\delta(\boldsymbol{x})$, using a fourth-order interpolation scheme, which has advantageous anti-aliasing properties that allow unbiased measurements up to the Nyquist frequency (Hockney & Eastwood 1981; Sefusatti et al. 2016). After Fourier transforming $\delta(\boldsymbol{x})$ to get $\delta(\boldsymbol{k})$, we measure the bispectrum monopole

$$B_0^g(k_1, k_2, k_3) = \frac{1}{V_B} \int_{k_1} \mathrm{d}^3 q_1 \int_{k_2} \mathrm{d}^3 q_2 \int_{k_3} \mathrm{d}^3 q_3 \, \delta_{\mathrm{D}}(\boldsymbol{q}_{123}) \, \delta(\boldsymbol{q}_1) \, \delta(\boldsymbol{q}_2) \, \delta(\boldsymbol{q}_3) - B_0^{\mathrm{SN}}. \tag{6}$$

δ_D is the Dirac delta function, V_B is the normalization factor proportional to the number of triplets that can be found in the k_1, k_2, k_3 triangle bin, and B_0^{SN} is the correction term for the Poisson shot noise. Throughout the paper, we use $\delta(\boldsymbol{x})$ grids with $N_{\mathrm{grid}} = 360$ and triangle configurations defined by k_1, k_2, k_3 bins of width $\Delta k = 3k_f = 0.01885 \, h/\mathrm{Mpc}$, where $k_f = 2\pi/(1000 \, h^{-1}\mathrm{Mpc})$.
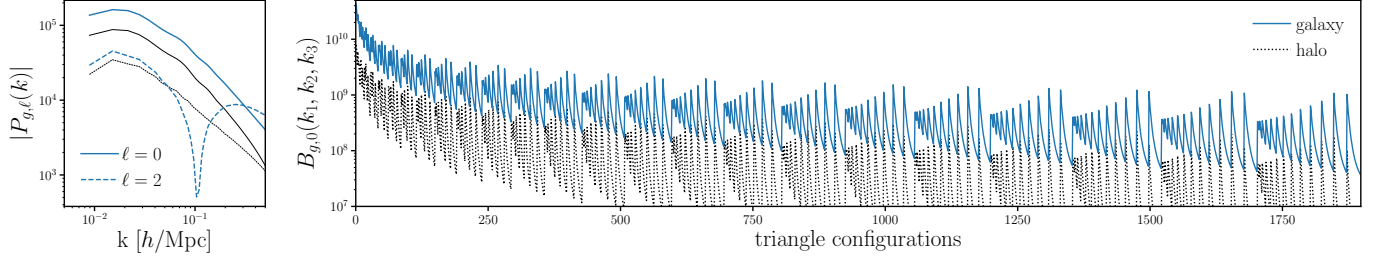
Figure 2. The redshift-space galaxy power spectrum multipoles ($P_0^g+P_2^g$; left) and bispectrum monopole (B_0^g; right) of the fiducial HOD galaxy catalog (blue). The $P_0^g+P_2^g$ and B_0^g are averaged over one set of HOD realizations run on 15,000 N-body QUIJOTE simulations measured using the same FFT-based estimator as Hahn et al. (2020). In the left panel, we plot both the power spectrum monopole ($\ell = 0$; solid) and quadrupole ($\ell = 2$; dashed). In the right panel, we plot B_0^g for all 1898 triangle configurations with $k_1, k_2, k_3 \leq k_{\max} = 0.5\,h/\text{Mpc}$. The configurations are ordered by looping through k_3 in the inner most loop and k_1 in the outer most loop satisfying $k_1 \leq k_2 \leq k3$. We include for comparison the Hahn et al. (2020) halo P_ℓ^h and B_0^h at the fiducial cosmology (black).

In Figure 2, we present the redshift-space galaxy power spectrum multipoles ($P_0^g+P_2^g$; left) and bispectrum (B_0^g; right) of the fiducial HOD galaxy catalog (blue). The $P_0^g+P_2^g$ and B_0^g are averaged over one set of HOD realizations run on 15,000 N-body QUIJOTE simulations at the fiducial cosmology. In the left panel, we plot both the power spectrum monopole ($\ell = 0$; solid) and quadrupole ($\ell = 2$; dashed). In the right panel, we plot B_0^g for all 1898 triangle configurations with $k_1, k_2, k_3 \leq k_{\max} = 0.5\,h/\text{Mpc}$. The configurations are ordered by looping through k_3 in the innermost loop and k_1 in the outer-most loop satisfying $k_1 \leq k_2 \leq k_3$. For comparison, we include the redshift-space halo power spectrum and bispectrum at the fiducial cosmology from Hahn et al. (2020) (black dotted).

To estimate the constraining power of $P_0^g+P_2^g$ and B_0^g, we use Fisher information matrices, which have been ubiquitously used in cosmology (*e.g.* Jungman et al. 1996; Tegmark et al. 1997; Dodelson 2003; Heavens 2009; Verde 2010):

$$F_{ij} = -\left\langle \frac{\partial^2 \ln \mathcal{L}}{\partial \theta_i \partial \theta_j} \right\rangle, \tag{7}$$

As in Hahn et al. (2020), we assume that the B_0^g likelihood is Gaussian and neglect the covariance derivative term (Carron 2013) and estimate the Fisher matrix as

$$F_{ij} = \frac{1}{2}\, \text{Tr}\left[\boldsymbol{C}^{-1} \left(\frac{\partial B_0^g}{\partial \theta_i} \frac{\partial B_0^{g\,T}}{\partial \theta_j} + \frac{\partial B_0^{g\,T}}{\partial \theta_i} \frac{\partial B_0^g}{\partial \theta_j} \right) \right]. \tag{8}$$

We derive the covariance matrix, $\boldsymbol{C}$, using 15,000 fiducial galaxy catalogs. The derivatives along the cosmological and HOD parameters, $\partial B_0^g / \partial \theta_i$, are estimated using finite difference. For all parameters other than M_ν, we estimate

$$\frac{\partial B_0^g}{\partial \theta_i} \approx \frac{B_0^g(\theta_i^+) - B_0^g(\theta_i^-)}{\theta_i^+ - \theta_i^-}, \tag{9}$$

Table 2. Marginalized Fisher parameter constraints from the redshift-space $P_0^g + P_2^g$, B_0^g, and $P_0^g + P_2^g + B_0^g$. We list constraints for cosmological parameters M_ν, Ω_m, Ω_b, h, n_s, and σ_8 as well as HOD and nuisance parameters.

	$k_{\max} = 0.2\ h/\text{Mpc}$			$k_{\max} = 0.5\ h/\text{Mpc}$		
	$P_0^g + P_2^g$	B_0^g	$P_0^g + P_2^g + B_0^g$	$P_0^g + P_2^g$	B_0^g	$P_0^g + P_2^g + B_0^g$
M_ν	0.795 (0.132)	0.313 (0.123)	0.282 (0.098)	0.334 (0.112)	0.073 (0.055)	0.071 (0.048)
Ω_m	0.061 (0.021)	0.047 (0.021)	0.030 (0.014)	0.037 (0.017)	0.018 (0.012)	0.013 (0.008)
Ω_b	0.027 (0.002)	0.017 (0.002)	0.013 (0.001)	0.015 (0.002)	0.006 (0.001)	0.005 (0.001)
h	0.351 (0.014)	0.204 (0.014)	0.157 (0.010)	0.178 (0.011)	0.052 (0.008)	0.047 (0.006)
n_s	0.427 (0.005)	0.230 (0.005)	0.165 (0.005)	0.206 (0.005)	0.053 (0.005)	0.049 (0.004)
σ_8	0.209 (0.029)	0.116 (0.027)	0.053 (0.023)	0.089 (0.025)	0.034 (0.014)	0.021 (0.012)
$\log M_{\min}$	1.435 (1.061)	0.499 (0.442)	0.335 (0.210)	0.457 (0.258)	0.114 (0.100)	0.089 (0.070)
$\sigma_{\log M}$	3.072 (2.390)	1.090 (0.926)	0.712 (0.506)	0.963 (0.655)	0.215 (0.204)	0.174 (0.140)
$\log M_0$	2.257 (1.845)	1.387 (1.341)	0.431 (0.386)	0.547 (0.361)	0.261 (0.232)	0.088 (0.079)
α	0.749 (0.592)	0.309 (0.294)	0.170 (0.167)	0.257 (0.180)	0.082 (0.073)	0.034 (0.033)
$\log M_1$	0.819 (0.691)	0.434 (0.408)	0.244 (0.149)	0.193 (0.119)	0.115 (0.113)	0.071 (0.056)

[*] constraints with *Planck* priors in parentheses

where $B_0^g(\theta_i^+)$ and $B_0^g(\theta_i^-)$ are the average bispectrum of the (500 simulations) $\times$ (3 RSD axes) $\times$ (5 HOD realizations) $= 7,500$ realizations at θ_i^+ and θ_i^-, the HOD or cosmological parameter values above and below the fiducial parameters. For M_ν, where the fiducial value is 0.0 eV, we use the galaxy catalogs at M_ν^+, M_ν^{++}, $M_\nu^{+++} = 0.1, 0.2, 0.4$ eV (Table 1) to estimate

$$\frac{\partial B_0^g}{\partial M_\nu} \approx \frac{-21 B_0^g(\theta_{\text{fid}}^{\text{ZA}}) + 32 B_0^g(M_\nu^+) - 12 B_0^g(M_\nu^{++}) + B_0^g(M_\nu^{+++})}{1.2}, \tag{10}$$

which provides a $\mathcal{O}(\delta M_\nu^2)$ order approximation. Since the simulations at M_ν^+, M_ν^{++}, and M_ν^{+++} are generated from Zel'dovich initial conditions, we use simulations at the fiducial cosmology also generated from Zel'dovich initial conditions ($\theta_{\text{fid}}^{\text{ZA}}$). Our simulation-based approach with galaxy catalogs constructed from N-body simulations is essential for accurately quantifying the constraining power of the bispectrum beyond the limitations of analytic methods down to nonlinear regimes.

5. RESULTS

We present the Fisher matrix constraints for M_ν and other cosmological parameters from the redshift-space galaxy $P_0^g + P_2^g$ (blue), B_0^g (green), and combined $P_0^g + P_2^g + B_0^g$ (orange) in Figure 3. These constraints marginalize over the Zheng et al. (2007) HOD parameters (bottom panels) and extends to $k_{\max} = 0.5\,h/\text{Mpc}$. The contours mark the 68% and 95% confidence intervals. With the redshift-space $P_0^g + P_2^g$ alone, we derive the following 1σ constraints for $\{\Omega_\text{m}, \Omega_\text{b}, h, n_s, \sigma_8, M_\nu\}$: 0.037, 0.015, 0.178, 0.206, 0.089, and 0.334 eV. With the redshift-space B_0^g alone, and for only a
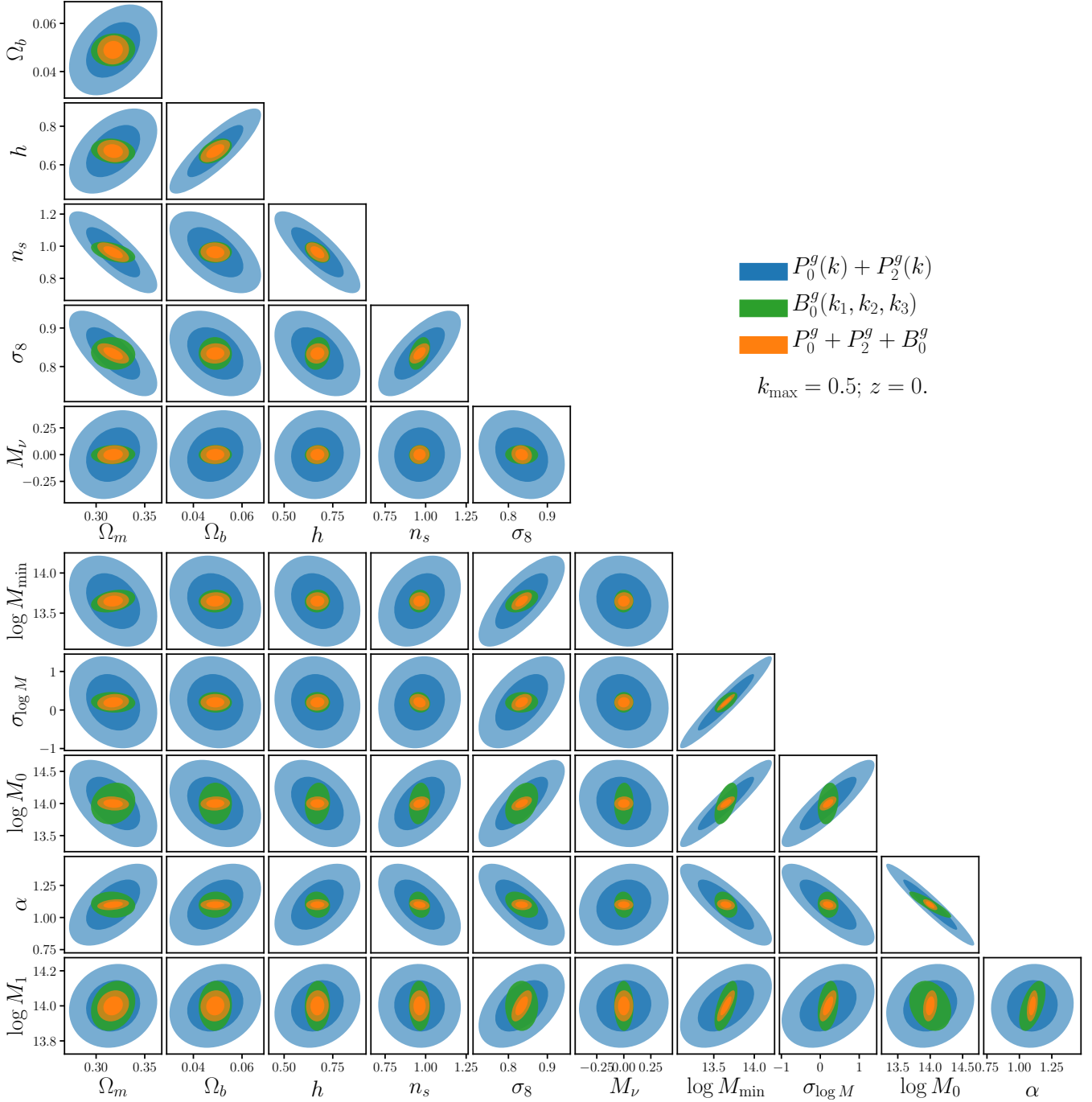
Figure 3. Fisher matrix constraints for M_ν and other cosmological parameters for the redshift-space galaxy $P_0^g + P_2^g$ (blue), B_0^g (green), and combined $P_0^g + P_2^g$ and B_0^g (orange) for $k_{max} = 0.5\,h/\mathrm{Mpc}$, for a $1(\mathrm{Gpc}/h)^3$ volume. Our forecasts marginalizes over the Zheng et al. (2007) HOD parameters: $\log M_{min}, \sigma_{\log M}, \log M_0, \alpha$, and $\log M_1$ (bottom panels). The contours mark the 68% and 95% confidence intervals. The bispectrum substantially improves constraints on all of the cosmological parameters over the power spectrum. Ω_m, Ω_b, h, n_s, and σ_8 constraints improve by factors of 2.8, 3.1, 3.8, 4.2, and 4.2, respectively. For M_ν, the bispectrum improves σ_{M_ν} from 0.3344 to 0.0706 eV — over a factor of $\sim$5 improvement over the power spectrum.
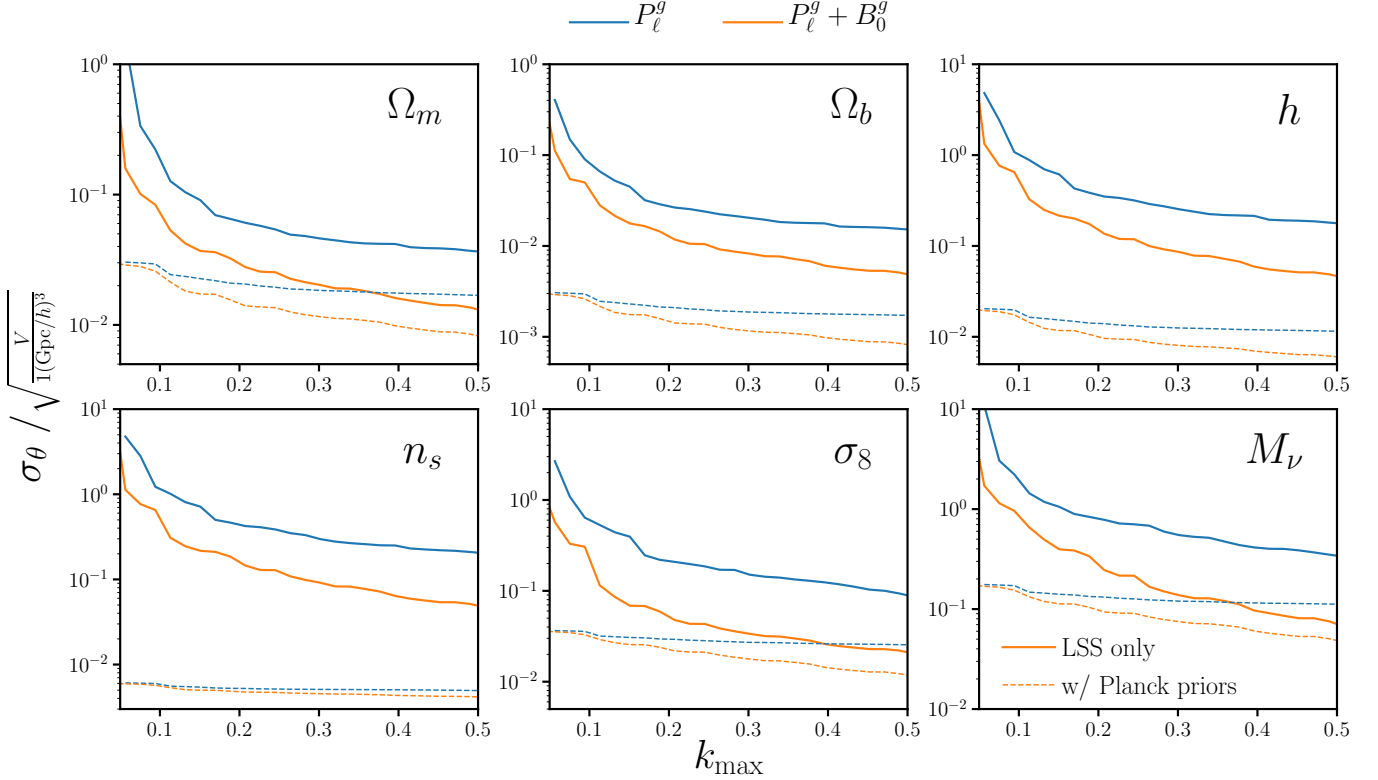
Figure 4. Marginalized 1σ constraints, σ_θ, of the cosmological parameters Ω_m, Ω_b, h, n_s, σ_8, and M_ν as a function of $k_{\max}$ for the redshift-space $P_0^g + P_2^g$ (blue) and combined $P_0^g + P_2^g + B_0^g$ (orange). Even after marginalizing over HOD parameters, the galaxy bispectrum *significantly* improves cosmological parameter constraints *For $k_{\max} = 0.2$ and $0.5\,h/$Mpc, including the bispectrum improves $\{\Omega_m, \Omega_b, h, n_s, \sigma_8, M_\nu\}$ constraints by factors of $\{2.0, 2.0, 2.2, 2.6, 3.9, 2.8\}$ and $\{2.8, 3.1, 3.8, 4.2, 4.2, 4.7\}$.* When we include *Planck* priors (dotted), the improvement from B_0^g is even more evident. The constraining power of $P_0^g + P_2^g$ completely saturates for $k_{\max} \gtrsim 0.12\,h/$Mpc. Adding B_0^g not only improves constraints, but the constraints continue to improve for higher $k_{\max}$. At $k_{\max} = 0.2$ and $0.5\,h/$Mpc, the $P_0^g + P_2^g + B_0^g$ improves the M_ν constraint by 1.4 and 2.3× over $P_0^g + P_2^g$. We emphasize that the constraints above are for 1 (Gpc/h)³ box and thus underestimate the constraining power of upcoming galaxy clustering surveys.

$1(\text{Gpc}/h)^3$ volume, we get: 0.018, 0.006, 0.052, 0.053, 0.034, and 0.073 eV. *The galaxy bispectrum achieves significantly tighter constraints on all cosmological parameters over the power spectrum.*

Furthermore, we find that by combining $P_0^g + P_2^g$ and B_0^g produces even better constraints by breaking a number of parameter degeneracies. Among the cosmological parameters, in addition to breaking the $\sigma_8 - M_\nu$ degeneracy, which limits power spectrum analyses, the $\Omega_m - \sigma_8$ degeneracy is also broken and leads to significant improvements in both Ω_m and σ_8 constraints. Meanwhile, for the HOD parameters, degeneracies with $\log M_0$, α, and $\log M_1$ are all substantially reduced. Combining $P_0^g + P_2^g$ and B_0^g, we get the following 1σ constraints for Ω_m, Ω_b, h, n_s, σ_8, and M_ν: 0.013, 0.005, 0.047, 0.049, 0.021, and 0.071. *With $P_0^g + P_2^g$ and B_0^g combined, we improve Ω_m, Ω_b, h, n_s, and σ_8*

constraints by factors of 2.8, 3.1, 3.8, 4.2, and 4.2; M_ν constraint improves by a factor of 4.7 over the $P_0^g + P_2^g$ constraints

In Figure 4, we present the marginalized 1σ constraints of the cosmological parameters Ω_m, Ω_b, h, n_s, σ_8, and M_ν as a function of k_{max}, $\sigma_\theta(k_{max})$, for $P_0^g + P_2^g$ (blue) and the combined $P_0^g + P_2^g + B_0^g$ (orange). Again, these constraints marginalize over the Zheng et al. (2007) HOD parameters. For both $P_0^g + P_2^g$ and $P_0^g + P_2^g + B_0^g$, parameter constraints expectedly improve as we include smaller scales (higher k_{max}). More importantly, Figure 4 highlights that *the galaxy bispectrum significantly improves cosmological parameter constraints*. Even for $k_{max} \sim 0.2\,h/\mathrm{Mpc}$, including B_0^g improves Ω_m, Ω_b, h, n_s, σ_8 and M_ν constraints by factors of 2.0, 2.0, 2.2, 2.6, 3.9, and 2.8.

In Figure 4, we also present $\sigma_\theta(k_{max})$ for $P_0^g + P_2^g$ (blue dashed) and $P_0^g + P_2^g + B_0^g$ (orange dashed) *with priors from Planck*. Once we include *Planck* priors, $P_0^g + P_2^g$ constraints do not significantly improve beyond $k_{max} \gtrsim 0.12\,h/\mathrm{Mpc}$. On the other hand, the constraints from $P_0^g + P_2^g + B_0^g$ continue to improve throughout the k_{max} range. At $k_{max} = 0.2\,h/\mathrm{Mpc}$, B_0^g improves the $P_0^g + P_2^g + Planck$ priors constraints on Ω_m, Ω_b, h, n_s, σ_8 and M_ν constraint by factors of 1.4, 1.4, 1.4, 1.1, 1.3, and 1.4×; at $k_{max} = 0.5\,h/\mathrm{Mpc}$, B_0^g improves the $P_0^g + P_2^g + Planck$ priors constraints by factors of 2.0, 2.1, 1.9, 1.2, 2.2, and 2.3×. Hence, even with *Planck* priors, the galaxy bispectrum significantly improves cosmological constraints. In fact, since our constraints are for a 1 $(\mathrm{Gpc}/h)^3$ box, for upcoming galaxy redshift surveys (*e.g.* DESI, Euclid), which will probe a much larger volume, we expect larger contributions to the constraining power from galaxy clustering and, thus, greater improvements from including B_0^g even with *Planck* priors.

In the previous paper of the series (Hahn et al. 2020), we presented the full information content of the redshift-space halo bispectrum, B_0^h. For B_0^h to $k_{max} = 0.5\,h/\mathrm{Mpc}$, Hahn et al. (2020) derived 1σ constraints of 0.012, 0.004, 0.04, 0.036, 0.014, and 0.057 for Ω_m, Ω_b, h, n_s, σ_8 and M_ν. B_0^g produces overall broader constraints on the cosmological parameters (Table 2). This is the same for $k_{max} = 0.2\,h/\mathrm{Mpc}$. A comparison of the signal-to-noise ratios (SNR) of B_0^g and B_0^h, estimated from the covariance matrix (*e.g.* Sefusatti & Scoccimarro 2005; Sefusatti et al. 2006; Chan & Blot 2017), also confirm the lower constraining power of B_0^g. Furthermore, while both B_0^h and B_0^g SNRs increase at higher k_{max}, the increase is lower for B_0^g than B_0^h. Marginalizing over HOD parameters reduces some of the constraining power of the bispectrum. Fingers-of-god (FoG), the elongation of satellite galaxies in redshift-space along the line-of-sight due to their virial velocities inside halos, also contributes to this reduction. Nevertheless, B_0^g significantly improves parameter constraints over $P_0^g + P_2^g$. In fact, marginalizing over HOD parameters and FoG reduces the constraining power of the power spectrum more than the bispectrum. Therefore, *we find larger improvements in the parameter constraints from B_0^g over $P_0^g + P_2^g$ than from B_0^h over P_ℓ^h.*

5.1. *Comparison to Previous Works*

Other previous works have also quantified the information content of the bispectrum: (*e.g.* Scoccimarro et al. 2004; Sefusatti et al. 2006; Sefusatti & Komatsu 2007; Song et al. 2015; Tellarini et al. 2016; Yamauchi et al. 2017; Karagiannis et al. 2018; Yankelevich & Porciani 2019; Chudaykin & Ivanov 2019; Coulton et al. 2019; Reischke et al. 2019; Agarwal et al. 2020). We focus our comparison to Sefusatti et al. (2006), Yankelevich & Porciani (2019), Agarwal et al. (2020) and Chudaykin &

Ivanov (2019), which provide bispectrum forecasts for full sets of cosmological parameters. Sefusatti et al. (2006) present ΛCDM forecasts for a joint likelihood analysis of B_0^g with P^g and WMAP. For $k_{\max} = 0.2\,h/\mathrm{Mpc}$, they find that including B_0^g improves constraints on Ω_{m}, Ω_{b}, h, n_s, and σ_8 by 1.6, 1.2, 1.5, 1.4, and 1.5 times from the P^g and WMAP constraints. In comparison, for $k_{\max} = 0.2\,h/\mathrm{Mpc}$ and with *Planck* priors, we find B_0^g improves constraints by 1.5, 1.4, 1.4, 1.1, and 1.3$\times$, which is in good agreement. There are, however, some significant differences between our analyses. First, Sefusatti et al. (2006) uses the WMAP likelihood while we use priors from *Planck*. Furthermore, in our simulation-based approach, we marginalize over the HOD parameters whereas Sefusatti et al. (2006) marginalize over the linear and quadratic bias terms (b_1, b_2) in their perturbation theory approach. Nevertheless, our results are consistent with the improvement Sefusatti et al. (2006) find in parameter constraints with B_0^g.

Next, Yankelevich & Porciani (2019) present ΛCDM, wCDM and $w_0 w_a$CDM Fisher forecasts for a Euclid-like survey (Laureijs et al. 2011) over $0.65 < z < 2.05$. Focusing only on their ΛCDM forecasts, they find that for $k_{\max} = 0.15\,h/\mathrm{Mpc}$, $P^g + B_0^g$ produces constraints on Ω_{cdm}, Ω_{b}, A_s, h, n_s that are $\sim 1.3\times$ tighter than P^g alone. In contrast, we find even at $k_{\max} = 0.15\,h/\mathrm{Mpc}$ significantly larger improvement in the parameter constraints from including B_0^g. We note that Yankelevich & Porciani (2019) present forecasts for a significantly different galaxy sample. For instance, their $z = 0.7$ redshift bin has $\bar{n}_g = 2.76 \times 10^{-3}\,h^3\mathrm{Gpc}^{-3}$ and linear bias of $b_g = 1.18$. Meanwhile our galaxy sample is at $z = 0$ with $\bar{n}_g \sim 1.63 \times 10^{-4}\,h^3\mathrm{Gpc}^{-3}$ and linear bias of $b_g \sim 2.55$ (Section 3). Furthermore, while we use the HOD framework, they use a bias expansion with linear, non-linear, and tidal bias (b_1, b_2, and b_{s^2}). They also marginalize over 56 nuisance parameters since they jointly analyze 14 z bins, each with 4 nuisance parameters. Lastly, Yankelevich & Porciani (2019) use perturbation theory models and, therefore, limit their forecast to $k_{\max} = 0.15\,h/\mathrm{Mpc}$ due to theoretical uncertainties. Despite the differences, when they estimate the constraining power beyond $k_{\max} > 0.15\,h/\mathrm{Mpc}$ using Figure of Merit they find that the constraining power of B_0^g relative to P^g increases for higher $k_{\max}$ consistent with our results.

Similar to Yankelevich & Porciani (2019), Agarwal et al. (2020) present ΛCDM Fisher forecasts for a Euclid-like survey. They use effective field theory based PT to model the 1-loop galaxy power spectrum and tree-level galaxy bispectrum, which requires 22 parameters that include 5 galaxy bias parameters and 9 selection parameters. Based on the limitations of their PT model, they probe P_g down to $k_{\max} = 0.35$ and B_g down to $k_{\max} 0.1\,h/\mathrm{Mpc}$. For fixed selection parameters, which account for selection effects, they find $> 2\times$ tighter cosmological parameter constraints from including B_g. Marginalizing over selection parameters, they find $> 4\times$ tighter constraints. These improvements are roughly consistent with our improvement from B_0^g. Overall, Agarwal et al. (2020) find significantly larger improvements in the cosmological parameter from including the bispectrum than Yankelevich & Porciani (2019). Agarwal et al. (2020) primarily attribute this difference to their less conservative galaxy bias model and argue that using 56 nuisance parameters (Yankelevich & Porciani 2019) is too conservative and ignores the expected redshift dependent continuity of the galaxy bias parameters.

Finally, Chudaykin & Ivanov (2019) present $M_\nu + \Lambda$CDM forecasts for the power spectrum and bispectrum of a Euclid-like survey over $0.5 < z < 2.1$. For ω_{cdm}, ω_b, h, n_s, A_s, and M_ν they

find $\sim 1.2, 1.5, 1.4, 1.3$, and $1.1\times$ tighter constraints from $P_0^g + P_2^g$ and B_0^g than from $P_0^g + P_2^g$ alone. For M_ν, they find a factor of 1.4 improvement, from 0.038 eV to 0.028 eV. With *Planck*, they get $\sim 2, 1.1, 2.3, 1.5, 1.1$, and $1.3\times$ tighter constraints for $\omega_{\rm cdm}$, ω_b, h, n_s, A_s, and M_ν from including B_0^g. Overall, Chudaykin & Ivanov (2019) find significant improvements from including B_0^g — consistent with our results. However, they find more modest improvements. Again, there are significant differences between our analyses. First, like Yankelevich & Porciani (2019) and Agarwal et al. (2020), Chudaykin & Ivanov (2019) present forecasts for a Euclid-like survey, which is significantly different than our galaxy sample. Their $z = 0.6$ redshift bin, for instance, has $\bar{n}_g = 3.83 \times 10^{-3}\ h^3{\rm Gpc}^{-3}$ and linear bias of $b_g = 1.14$. Next, they include the Alcock-Paczynski (AP) effect for $P_0^g + P_2^g$ but not for B_0^g. They find that including the AP effect significantly improves $P_0^g + P_2^g$ constraints (e.g. tightens M_ν constraints by $\sim 30\%$); this reduces the improvement they report from including B_0^g.

Another difference between our analyses is that although Chudaykin & Ivanov (2019) use a more accurate Markov-Chain Monte-Carlo (MCMC) approach to derive parameter constraints, they neglect the non-Gaussian contributions to both $P_0^g + P_2^g$ and B_0^g covariance matrices and also do not include the covariance between $P_0^g + P_2^g$ and B_0^g for the joint constraints. We find that neglecting the off-diagonal terms of the covariance overestimates 1σ M_ν constraints by 25% for our $k_{\rm max} = 0.2\,h/{\rm Mpc}$ constraints. Lastly, Chudaykin & Ivanov (2019) use a one-loop and tree-level perturbation theory to model $P_0^g + P_2^g$ and B_0^g, respectively. Rather than imposing a $k_{\rm max}$ cutoff to restrict their forecasts to scales where their perturbation theory models can be trusted, they use a theoretical error covariance model approach from Baldauf et al. (2016). With a tree-level B_0^g model, theoretical errors quickly dominate at $k_{\rm max} \gtrsim 0.1\,h/{\rm Mpc}$, where one- and two-loop contribute significantly (*e.g.* Lazanu & Liguori 2018). So effectively, their forecasts do not include the constraining power on those scales. If we restrict our forecast to $k_{\rm max} = 0.25\,h/{\rm Mpc}$ for $P_0^g + P_2^g$ and $k_{\rm max} = 0.1\,h/{\rm Mpc}$ for B_0^g, our $\Omega_{\rm m}$, $\Omega_{\rm b}$, h, n_s, σ_8, and M_ν constraints improve by 1.2, 1.2, 1.2, 1.4, 1.8, and $1.3\times$ from including B_0^g, roughly consistent with Chudaykin & Ivanov (2019).

5.2. *Forecast Caveats*

Among the various differences between our forecast and previous works, we emphasize that we use a simulation-based approach. This allows us to go beyond previous perturbation theory models and accurately quantify the constraining power in the nonlinear regime. A simulation-based approach, however, has a few caveats. First, our forecasts rely on the stability and convergence of the covariance matrix and numerical derivatives. For our constraints, we use a total of $75{,}000$ galaxy catalogs (Section 3): $15{,}000$ for the covariance matrices and $60{,}000$ for the derivatives with respect to 11 parameters ($7{,}500$ at each parameter). To ensure the robustness of our results, we conduct the same set of convergence tests as Hahn et al. (2020). First, we test whether our results have sufficiently converged by deriving the constraints using different numbers of galaxy catalogs to estimate the covariance matrix and derivatives: $N_{\rm cov}$ and $N_{\rm deriv}$. For $N_{\rm cov}$, we find $< 0.5\%$ variation in σ_θ for $N_{\rm cov} > 12{,}000$. For $N_{\rm deriv}$, we find $< 10\%$ variation σ_θ for $N_{\rm cov} > 6{,}000$. Since we have sufficient $N_{\rm cov}$ and $N_{\rm deriv}$, we conclude that our constraints are not impacted by the convergence of the covariance matrix or derivatives — especially to the accuracy level of Fisher forecasting.

Besides the convergence of the numerical derivatives, the M_ν derivatives can be evaluated using different sets of cosmologies. In our analysis, we evaluate $\partial P_0^g + P_2^g / \partial M_\nu$ and $\partial B_0^g / \partial M_\nu$ using simulations at the $\{\theta_{\rm ZA}, M_\nu^+, M_\nu^{++}, M_\nu^{+++}\}$ cosmologies. They can, however, also be estimated using two other sets of cosmologies: (i) $\{\theta_{\rm ZA}, M_\nu^+\}$ and (ii) $\{\theta_{\rm ZA}, M_\nu^+, M_\nu^{++}\}$. Replacing $\partial P_0^g + P_2^g / \partial M_\nu$ and $\partial B_0^g / \partial M_\nu$ estimates of our forecast with derivatives estimated using (i) or (ii) does not impact $\Omega_{\rm m}$, $\Omega_{\rm b}$, h, n_s, and σ_8 constraints. Although the different derivatives impact M_ν constraints, they impact both $P_0^g + P_2^g$ and B_0^g forecasts by a similar factor so the improvement from including B_0^g is not impacted. For our fiducial HOD, we chose parameter values based on Zheng et al. (2007) fits to the SDSS $M_r < -21.5$ and -22 samples, except for the tighter scatter $\sigma_{\log M} = 0.2$ dex — due to the halo mass limit of QUIJOTE (Section 3). As a result, our HOD galaxy catalogs have a different selection function than observed samples, typically selected based on M_r or M_* cuts (*e.g.* SDSS or BOSS). To estimate the impact of our fiducial $\sigma_{\log M}$ choice, we repeat our forecasts but using $\partial P_0^g + P_2^g / \partial \sigma_{\log M}$ and $\partial B_0^g / \partial \sigma_{\log M}$ at $\sigma_{\log M} = 0.55$ dex. These derivatives are estimated using the higher resolution QUIJOTE simulation, which have $8\times$ the mass resolution but only 100 realizations (Villaescusa-Navarro et al. 2019). The change in $\partial P_0^g + P_2^g / \partial \sigma_{\log M}$ and $\partial B_0^g / \partial \sigma_{\log M}$ significantly impacts the HOD parameter constraints; however, it has a *negligible* effect on the cosmological parameter constraints.

Besides convergence and stability, our forecasts are derived from Fisher matrices. We, therefore, assume that the posterior is approximately Gaussian. When posteriors are highly non-elliptical or asymmetric, Fisher forecasts significantly underestimate the constraints (Wolz et al. 2012). However, in this paper we do not derive actual parameter constraints from observations but focus on quantifying the information content and constraining power of B_0^g relative to $P_0^g + P_2^g$. Hence, we do not explore beyond the Fisher forecast. When we analyze the SDSS-III BOSS data using a simulation-based approach later in the series, we will use a robust method to sample the posterior.

In addition to the caveats above, a number of extra steps and complications remain between this work and a full galaxy bispectrum analysis. For instance, we use the standard Zheng et al. (2007) HOD model, which does not include assembly bias. While there is little evidence of assembly bias for a high luminosity galaxy sample (Zentner et al. 2016; Vakili & Hahn 2019; Beltz-Mohrmann et al. 2020), such as our fiducial HOD, many works have demonstrated that assembly bias impacts galaxy clustering for lower luminosity/mass samples both using observations (Pujol & Gaztañaga 2014; Hearin et al. 2016; Pujol et al. 2017; Zentner et al. 2019; Vakili & Hahn 2019; Obuljen et al. 2020) and hydrodynamic simulations (Chaves-Montero et al. 2016; Beltz-Mohrmann et al. 2020).

Central and satellite velocity biases, not included in the Zheng et al. (2007) HOD, can also impact galaxy clustering (Guo et al. 2015a,b). Central galaxies, both in observations and simulations, are not found to be at rest in the centers of the host halos (*e.g.* Berlind et al. 2003; Yoshikawa et al. 2003; van den Bosch et al. 2005; Skibba et al. 2011). Similarly, satellite galaxies in simulations do not have the same velocities as the underlying dark matter (*e.g.* Diemand et al. 2004; Gao et al. 2004; Lau et al. 2010; Munari et al. 2013; Wu & Huterer 2013). The central velocity bias reduces the Kaiser effect and the satellite velocity bias reduces the FoG effect; both can impact galaxy clustering. However, for the high luminosity SDSS samples, Guo et al. (2015b) find little satellite velocity bias. In simulations,

Beltz-Mohrmann et al. (2020) similarly find that removing central and satellite velocity biases in the Illustris-TNG and EAGLE simulations has little impact on various clustering measurements of high luminosity samples. Although assembly bias and velocity bias likely do not impact our forecasts, they must be included for lower luminosity/mass galaxy samples and for higher precision measurements of observations. Therefore, when we reanalyze BOSS with a simulation-based approach later in the series, we will use a decorated HOD framework (*e.g.* Hearin et al. 2016; Vakili & Hahn 2019; Zhai et al. 2019) that includes both assembly bias and velocity biases. Given the improvements we see in HOD parameter constraints from B_0^g in Figure 3, B_0^g also has the potential to better constrain the assembly bias parameters and improve our understanding of the galaxy-halo connection.

Our analysis also does not include baryonic effects. Although they have been typically neglected in galaxy clustering analyses, baryonic effects, such as feedback from active galactic nuclei (AGN), can impact the matter distribution at cosmological distances (*e.g.* White 2004; Zhan & Knox 2004; Jing et al. 2006; Rudd et al. 2008; Harnois-Déraps et al. 2015). For AGN feedback in particular, various works find an impact on the matter power spectrum (*e.g.* van Daalen et al. 2011; Vogelsberger et al. 2014; Hellwing et al. 2016; Peters et al. 2018; Springel et al. 2018; Chisari et al. 2018; van Daalen et al. 2020). Although there is no consensus on the magnitude of the effect, ultimately, a more effective AGN feedback increases the impact on the matter clustering (Barreira et al. 2019). In state-of-the-art hydrodynamical simulations, Foreman et al. (2019) find $\lesssim 1\%$ impact on the matter power spectrum at $k \lesssim 0.5\,h/\mathrm{Mpc}$. For the matter bispectrum, they find that the effect of baryons is peaked at $k = 3\,h/\mathrm{Mpc}$ and, similarly, a $\lesssim 1\%$ effect at $k \lesssim 0.5\,h/\mathrm{Mpc}$. Although there is growing evidence of baryon impacting the matter clustering, the effect is mainly found on scales smaller than what is probed by galaxy clustering analyses with spectroscopic redshift surveys. We, therefore, do not include baryonic effects in our forecasts and do not consider it further in the series.

In our forecasts, we use B_0^g with triangles defined in k_1, k_2, k_3 bins of width $\Delta k = 3k_f$ (Section 4). Gagrani & Samushia (2017) find that for the growth rate parameter bispectrum multipoles beyond the monopole have significant constraining power. Yankelevich & Porciani (2019), with figure-of-merit (FoM) estimates, also find significant information content beyond the monopole. Furthermore, Yankelevich & Porciani (2019) also find that coarser binning of the triangle configurations reduces the information content of the bispectrum: binning by $\Delta k = 3k_f$ has $\sim 10\%$ less constraining power than binning by $\Delta k = k_f$. While including higher order multipoles and increase the binning are straightforward to implement, they both increase the dimensionality of the data vector. B_0^g alone binned by $\Delta k = 3k_f$ already has 1898 dimensions. Including the bispectrum multipoles and increasing the binning would not be feasible for a full bispectrum analysis without the use of data compression (*e.g.* Byun et al. 2017; Gualdi et al. 2018, 2019b,a). Thus, in the next paper in the series, we present how data compression can be incorporated in a galaxy bispectrum analysis.

Lastly, our forecasts are derived using periodic boxes and do not consider a realistic geometry or radial selection function of galaxy surveys. A realistic selection function will smooth the triangle configuration dependence and degrade the constraining power of the bispectrum (Sefusatti & Scoccimarro 2005). Furthermore, galaxy samples selected based on photometric properties can also be impacted by, for instance, the alignment of galaxies to the large-scale tidal fields (Hirata 2009;

Krause & Hirata 2011; Martens et al. 2018; Obuljen et al. 2019). If unaccounted for, this effect can significantly bias the inferred cosmological parameters (Agarwal et al. 2020). Such effects, however, further underscore the importance of the bispectrum. Marginalizing over them dramatically reduces the constraining power of the power spectrum alone and necessitates the bispectrum to break parameter degeneracies to tightly constrain cosmological parameters. Besides selection effects, we also do not account for super-sample covariance, which may also impact our constraints (Hamilton et al. 2006; Sefusatti et al. 2006; Takada & Hu 2013; Li et al. 2018; Wadekar & Scoccimarro 2019). Since super-sample covariance affects the power spectrum as well, we still expect to find substantial improvements in cosmological parameter constraints from including the bispectrum, especially for M_ν.

6. SUMMARY

Tight constraints on the total mass of neutrinos, M_ν, inform particle physics beyond the Standard Model and can potentially distinguish between the 'normal' and 'inverted' neutrino mass hierarchies. The current tightest constraints come from measuring the impact of M_ν on the expansion history and the growth of cosmic structure in the Universe using cosmological observables — combinations of CMB with other cosmological probes. However, constraints from upcoming ground-based CMB experiments will be severely limited by the degeneracy between M_ν and τ, the optical depth of reionization. Meanwhile, measuring the M_ν imprint on the 3D clustering of galaxies provides a complementary and opportune avenue for improving M_ν constraints. Progress in modeling nonlinear structure formation of simulations and in new simulation-based approaches now enables us to tractably exploit the accuracy of N-body simulations to analyze galaxy clustering. Furthermore, in the next few years, upcoming surveys such as DESI, PFS, Euclid, and the Roman Space Telescope will probe unprecedented cosmic volumes with galaxy redshifts. Together, these development present the opportunity to go beyond traditional perturbation theory methods, unlock the information content in nonlinear clustering where the impact of M_ν is strongest, and tightly constrain M_ν and other cosmological parameters.

In Hahn et al. (2020), the previous paper of the series, we demonstrated that the bispectrum breaks parameter degeneracies (*e.g.* M_ν–σ_8 degeneracy) that serious limit M_ν constraints with traditional two-point clustering statistics. We also illustrated the substantial constraining power of the bispectrum in nonlinear regimes. Hahn et al. (2020), however, focused on the redshift-space halo bispectrum while constraints on M_ν will come from galaxy distributions. In this work, we extend the Hahn et al. (2020) bispectrum forecasts to include a realistic galaxy bias model. With our eyes set on simulation-based analyses, we use the halo occupation distribution (HOD) galaxy bias framework and construct the MOLINO suite—75,000 galaxy mock catalogs from the QUIJOTE N-body simulations. Using these mocks, we present for the first time the total information content and constraining power of the *redshift-space galaxy bispectrum* down to nonlinear regimes. More specifically, we find

- B_0^g substantial improves in cosmological parameter constraints — especially M_ν — even after marginalizing over galaxy bias through the HOD parameters. Combining $P_0^g + P_2^g$ and B_0^g further improves constraints by breaking several key parameter degeneracies. For $k_{\max}=0.5\,h/\mathrm{Mpc}$,

B_0^g improves constraints on $\Omega_{\rm m}$, $\Omega_{\rm b}$, h, n_s, and σ_8 by 2.8, 3.1, 3.8, 4.2, 4.2, and 4.7× over power spectrum. For M_ν, we achieve 5.6× tighter constraints with B_0^g.

- Even with priors from *Planck*, B_0^g significantly improves cosmological constraints. For $k_{\rm max}$=0.5 h/Mpc, including B_0^g achieves 2.0, 2.1, 1.9, 1.2, 2.2, and 2.3× tighter constraints on $\Omega_{\rm m}$, $\Omega_{\rm b}$, h, n_s, σ_8, and M_ν than with P_0^g+P_2^g and *Planck*. B_0^g also substantially improves constraints at mildly non-linear regimes: for $k_{\rm max} \sim 0.2\,h$/Mpc, B_0^g achieves 1.4 and 2.8× tighter M_ν constraints than P_0^g+P_2^g with and without *Planck* priors.

- B_0^g has substantial constraining power on non-linear regime beyond $k_{\rm max} > 0.2\,h$/Mpc. This makes B_0^g particularly valuable when we include *Planck* priors: the constraining power of P_0^g+P_2^g completely saturates at $k_{\rm max} \gtrsim 0.12\,h$/Mpc while with B_0^g, constraints improve out to $k_{\rm max} = 0.5\,h$/Mpc.

Overall, our results clearly demonstrate the significant advantages of the galaxy bispectrum for more precisely constraining cosmological parameters — especially M_ν. There are, however, a few caveats in our forecast. Fisher matrix forecasts assume that the posterior is approximately Gaussian and can overestimate the constraints for highly non-elliptical or asymmetric posteriors. We also do not consider realistic survey geometry, selection effects, or super-sample covariance. Lastly, we include galaxy bias through the standard Zheng et al. (2007) HOD model. Although, this model is sufficiently accurate for a high luminosity galaxy sample that we consider, for galaxy samples from upcoming surveys additional effects such as assembly bias and velocity biases will need to be included. While these effects will impact the constraining power of B_0^g, they also impact the constraining power of P^g. Hence, we nonetheless expect significant improvements from including the galaxy bispectrum.

There is, in fact, room for more optimism. All the constraints we present in this paper are for a 1 h^{-3}Gpc^3 volume and for a galaxy sample with number density $\bar{n}_g \sim 1.63 \times 10^{-4}\ h^3$Gpc^{-3}. Upcoming surveys will probe *vastly* larger cosmic volumes and with higher number densities. For instance, PFS will probe $\sim 9\ h^{-3}$Gpc^3 with $\sim$5× higher n_g at $z{\sim}1.3$ (Takada et al. 2014); DESI will probe $\sim$50 h^{-3}Gpc^3 and its Bright Galaxy Survey and LRG sample will have $\sim$20 and 3× higher n_g, respectively (DESI~Collaboration et al. 2016; Ruiz-Macias et al. 2020). Euclid and the Roman Space Telescope, space-based surveys, will expand these volumes to higher redshifts. Constraints *conservatively* scale as $\propto 1/\sqrt{V}$ with volume and higher $\bar{n}_g$ samples will achieve higher signal-to-noise. Combined with our results, this suggests that analyzing the galaxy bispectrum in upcoming surveys has the potential to tightly constrain M_ν with unprecedented precision.

Now that we have demonstrated the total information content and constraining power of B_0^g, in the following paper of this series we will address a major practical challenge for a B_0^g analysis — its large dimensionality. We will present how data compression can be used to reduce the dimensionality and tractably estimate the covariance matrix in a P_0^g+P_2^g and B_0^g analysis using a simulation-based approach. Afterward, we will conduct a fully simulation-based P_0^g+P_2^g and B_0^g reanalysis of SDSS-III BOSS. The series will ultimately culminate in extending this simulation-based P_0^g+P_2^g and B_0^g analysis to constrain M_ν using the DESI survey.

REFERENCES

Abazajian, K. N., Adshead, P., Ahmed, Z., et al. 2016, arXiv:1610.02743 [astro-ph, physics:gr-qc, physics:hep-ph, physics:hep-th], arXiv:1610.02743 [astro-ph, physics:gr-qc, physics:hep-ph, physics:hep-th]

Adamek, J., Durrer, R., & Kunz, M. 2017, arXiv:1707.06938 [astro-ph, physics:gr-qc], arXiv:1707.06938 [astro-ph, physics:gr-qc]

Agarwal, N., Desjacques, V., Jeong, D., & Schmidt, F. 2020, arXiv e-prints, 2007, arXiv:2007.04340

Agarwal, S., & Feldman, H. A. 2011, Monthly Notices of the Royal Astronomical Society, 410, 1647

Allison, R., Caucal, P., Calabrese, E., Dunkley, J., & Louis, T. 2015, Physical Review D, 92, 123535

Allys, E., Marchand, T., Cardoso, J.-F., et al. 2020, arXiv:2006.06298 [astro-ph], arXiv:2006.06298 [astro-ph]

Alpaslan, M., & Tinker, J. L. 2019, arXiv e-prints, 1911, arXiv:1911.04509

Archidiacono, M., Brinckmann, T., Lesgourgues, J., & Poulin, V. 2017, Journal of Cosmology and Astro-Particle Physics, 2017, 052

Audren, B., Lesgourgues, J., Bird, S., Haehnelt, M. G., & Viel, M. 2013, Journal of Cosmology and Astro-Particle Physics, 2013, 026

Baldauf, T., Mirbabayi, M., Simonović, M., & Zaldarriaga, M. 2016

Banerjee, A., & Abel, T. 2020, arXiv:2007.13342 [astro-ph], arXiv:2007.13342 [astro-ph]

Banerjee, A., & Dalal, N. 2016, Journal of Cosmology and Astro-Particle Physics, 2016, 015

Banerjee, A., Powell, D., Abel, T., & Villaescusa-Navarro, F. 2018, arXiv:1801.03906 [astro-ph], arXiv:1801.03906 [astro-ph]

Barreira, A., Nelson, D., Pillepich, A., et al. 2019, Monthly Notices of the Royal Astronomical Society, 488, 2079

Beltz-Mohrmann, G. D., Berlind, A. A., & Szewciw, A. O. 2020, Monthly Notices of the Royal Astronomical Society, 491, 5771

Benson, A. J., Cole, S., Frenk, C. S., Baugh, C. M., & Lacey, C. G. 2000, Monthly Notices of the Royal Astronomical Society, 311, 793

Berlind, A. A., & Weinberg, D. H. 2002, The Astrophysical Journal, 575, 587

Berlind, A. A., Weinberg, D. H., Benson, A. J., et al. 2003, The Astrophysical Journal, 593, 1

Beutler, F., Seo, H.-J., Saito, S., et al. 2017, Monthly Notices of the Royal Astronomical Society, 466, 2242

Bird, S., Viel, M., & Haehnelt, M. G. 2012, Monthly Notices of the Royal Astronomical Society, 420, 2551

Bonn, J., Eitel, K., Glück, F., et al. 2011, Physics Letters B, 703, 310

Boyle, A., & Komatsu, E. 2018, Journal of Cosmology and Astro-Particle Physics, 2018, 035

Brandbyge, J., Hannestad, S., Haugbølle, T., & Thomsen, B. 2008, Journal of Cosmology and Astro-Particle Physics, 08, 020

Brinckmann, T., Hooper, D. C., Archidiacono, M., Lesgourgues, J., & Sprenger, T. 2019, Journal of Cosmology and Astroparticle Physics, 2019, 059

Byun, J., Eggemeier, A., Regan, D., Seery, D., & Smith, R. E. 2017, Monthly Notices of the Royal Astronomical Society, 471, 1581

Carron, J. 2013, Astronomy & Astrophysics, 551, A88

Castorina, E., Carbone, C., Bel, J., Sefusatti, E., & Dolag, K. 2015, Journal of Cosmology and Astro-Particle Physics, 2015, 043

Chan, K. C., & Blot, L. 2017, Physical Review D, 96, arXiv:1610.06585

Chaves-Montero, J., Angulo, R. E., Schaye, J., et al. 2016, Monthly Notices of the Royal Astronomical Society, 460, 3100

Chisari, N. E., Richardson, M. L. A., Devriendt, J., et al. 2018, Monthly Notices of the Royal Astronomical Society, 480, 3962

Chudaykin, A., & Ivanov, M. M. 2019, arXiv:1907.06666 [astro-ph, physics:hep-ph], arXiv:1907.06666 [astro-ph, physics:hep-ph]

Conroy, C., Prada, F., Newman, J. A., et al. 2007, The Astrophysical Journal, 654, 153

Contreras, S., Angulo, R., & Zennaro, M. 2020, arXiv e-prints, 2005, arXiv:2005.03672

Cooray, A., & Sheth, R. 2002, Physics Reports, 372, 1

Coulton, W. R., Liu, J., Madhavacheril, M. S., Böhm, V., & Spergel, D. N. 2019, Journal of Cosmology and Astro-Particle Physics, 2019, 043

Dalal, N., Doré, O., Huterer, D., & Shirokov, A. 2008, Physical Review D, 77, arXiv:0710.4560

Davis, M., Efstathiou, G., Frenk, C. S., & White, S. D. M. 1985, The Astrophysical Journal, 292, 371

DESI˜Collaboration, Aghamousa, A., Aguilar, J., et al. 2016, arXiv:1611.00036 [astro-ph], arXiv:1611.00036 [astro-ph]

Diemand, J., Moore, B., & Stadel, J. 2004, Monthly Notices of the Royal Astronomical Society, 352, 535

Dodelson, S. 2003, Modern Cosmology

Drexlin, G., Hannen, V., Mertens, S., & Weinheimer, C. 2013, Advances in High Energy Physics

Emberson, J. D., Yu, H.-R., Inman, D., et al. 2017, Research in Astronomy and Astrophysics, 17, 085

Euclid Collaboration, Knabenhans, M., Stadel, J., et al. 2018, arXiv:1809.04695 [astro-ph], arXiv:1809.04695 [astro-ph]

Font-Ribera, A., McDonald, P., Mostek, N., et al. 2014, Journal of Cosmology and Astro-Particle Physics, 05, 023

Foreman, S., Coulton, W., Villaescusa-Navarro, F., & Barreira, A. 2019, arXiv e-prints, 1910, arXiv:1910.03597

Forero, D. V., Tórtola, M., & Valle, J. W. F. 2014, Physical Review D, 90, 093006

Fukuda, Y., Hayakawa, T., Ichihara, E., et al. 1998, Physical Review Letters, 81, 1562

Gagrani, P., & Samushia, L. 2017, Monthly Notices of the Royal Astronomical Society, 467, 928

Gao, L., Springel, V., & White, S. D. M. 2005, Monthly Notices of the Royal Astronomical Society, 363, L66

Gao, L., White, S. D. M., Jenkins, A., Stoehr, F., & Springel, V. 2004, Monthly Notices of the Royal Astronomical Society, 355, 819

Gerbino, M. 2018, arXiv e-prints, arXiv:1803.11545

Gonzalez-Garcia, M. C., Maltoni, M., & Schwetz, T. 2016, Nuclear Physics B, 908, 199

Gualdi, D., Gil-Marín, H., Manera, M., Joachimi, B., & Lahav, O. 2019a, Monthly Notices of the Royal Astronomical Society: Letters, arXiv:1901.00987

Gualdi, D., Gil-Marín, H., Schuhmann, R. L., et al. 2019b, Monthly Notices of the Royal Astronomical Society, 484, 3713

Gualdi, D., Manera, M., Joachimi, B., & Lahav, O. 2018, Monthly Notices of the Royal Astronomical Society, 476, 4045

Guo, H., Zheng, Z., Zehavi, I., et al. 2015a, Monthly Notices of the Royal Astronomical Society, 453, 4368

—. 2015b, Monthly Notices of the Royal Astronomical Society, 446, 578

Hadzhiyska, B., Bose, S., Eisenstein, D., Hernquist, L., & Spergel, D. N. 2020, Monthly Notices of the Royal Astronomical Society, 493, 5506

Hahn, C., Tinker, J. L., & Wetzel, A. 2019, arXiv:1910.01644 [astro-ph], arXiv:1910.01644 [astro-ph]

Hahn, C., Villaescusa-Navarro, F., Castorina, E., & Scoccimarro, R. 2020, Journal of Cosmology and Astroparticle Physics, 03, 040

Hamilton, A. J. S., Rimes, C. D., & Scoccimarro, R. 2006, Monthly Notices of the Royal Astronomical Society, 371, 1188

Harker, G., Cole, S., Helly, J., Frenk, C., & Jenkins, A. 2006, Monthly Notices of the Royal Astronomical Society, 367, 1039

Harnois-Déraps, J., van Waerbeke, L., Viola, M., & Heymans, C. 2015, Monthly Notices of the Royal Astronomical Society, 450, 1212

Hearin, A. P., Zentner, A. R., van den Bosch, F. C., Campbell, D., & Tollerud, E. 2016, Monthly Notices of the Royal Astronomical Society, 460, 2552

Heavens, A. 2009, arXiv:0906.0664 [astro-ph], arXiv:0906.0664 [astro-ph]

Heitmann, K., Higdon, D., White, M., et al. 2009, The Astrophysical Journal, 705, 156

Hellwing, W. A., Schaller, M., Frenk, C. S., et al. 2016, Monthly Notices of the Royal Astronomical Society, 461, L11

Hirata, C. M. 2009, Monthly Notices of the Royal Astronomical Society, 399, 1074

Hockney, R. W., & Eastwood, J. W. 1981, Computer Simulation Using Particles

Jing, Y. P., Zhang, P., Lin, W. P., Gao, L., & Springel, V. 2006, The Astrophysical Journal Letters, 640, L119

Jungman, G., Kamionkowski, M., Kosowsky, A., & Spergel, D. N. 1996, Physical Review D, 54, 1332

Karagiannis, D., Lazanu, A., Liguori, M., et al. 2018, Monthly Notices of the Royal Astronomical Society, 478, 1341

Krause, E., & Hirata, C. M. 2011, Monthly Notices of the Royal Astronomical Society, 410, 2730

Kwan, J., Heitmann, K., Habib, S., et al. 2015, The Astrophysical Journal, 810, 35

Lacerna, I., Padilla, N., & Stasyszyn, F. 2014, Monthly Notices of the Royal Astronomical Society, 443, 3107

Lange, J. U., van den Bosch, F. C., Zentner, A. R., et al. 2019, arXiv:1909.03107 [astro-ph], arXiv:1909.03107 [astro-ph]

Lau, E. T., Nagai, D., & Kravtsov, A. V. 2010, The Astrophysical Journal, 708, 1419

Laureijs, R., Amiaux, J., Arduini, S., et al. 2011, arXiv e-prints, arXiv:1110.3193

Lazanu, A., & Liguori, M. 2018, Journal of Cosmology and Astro-Particle Physics, 2018, 055

Leauthaud, A., Tinker, J., Bundy, K., et al. 2012, The Astrophysical Journal, 744, 159

Lesgourgues, J., & Pastor, S. 2012

—. 2014

Li, Y., Schmittfull, M., & Seljak, U. 2018, Journal of Cosmology and Astro-Particle Physics, 2018, 022

Liu, A., Pritchard, J. R., Allison, R., et al. 2016, Physical Review D, 93, 043013

Mandelbaum, R., Seljak, U., Kauffmann, G., Hirata, C. M., & Brinkmann, J. 2006, Monthly Notices of the Royal Astronomical Society, 368, 715

Martens, D., Hirata, C. M., Ross, A. J., & Fang, X. 2018, Monthly Notices of the Royal Astronomical Society, 478, 711

Marulli, F., Carbone, C., Viel, M., Moscardini, L., & Cimatti, A. 2011, Monthly Notices of the Royal Astronomical Society, 418, 346

Massara, E., Villaescusa-Navarro, F., Ho, S., Dalal, N., & Spergel, D. N. 2020, arXiv:2001.11024 [astro-ph], arXiv:2001.11024 [astro-ph]

McClintock, T., Rozo, E., Becker, M. R., et al. 2018, arXiv:1804.05866 [astro-ph], arXiv:1804.05866 [astro-ph]

More, S., van den Bosch, F. C., Cacciato, M., et al. 2011, Monthly Notices of the Royal Astronomical Society, 410, 210

Munari, E., Biviano, A., Borgani, S., Murante, G., & Fabjan, D. 2013, Monthly Notices of the Royal Astronomical Society, 430, 2638

Navarro, J. F., Frenk, C. S., & White, S. D. M. 1997, The Astrophysical Journal, 490, 493

Obuljen, A., Dalal, N., & Percival, W. J. 2019, Journal of Cosmology and Astroparticle Physics, 10, 020

Obuljen, A., Percival, W. J., & Dalal, N. 2020, arXiv e-prints, 2004, arXiv:2004.07240

Peacock, J. A., & Smith, R. E. 2000, Monthly Notices of the Royal Astronomical Society, 318, 1144

Peters, A., Brown, M. L., Kay, S. T., & Barnes, D. J. 2018, Monthly Notices of the Royal Astronomical Society, 474, 3173

Petracca, F., Marulli, F., Moscardini, L., et al. 2016, Monthly Notices of the Royal Astronomical Society, 462, 4208

Planck Collaboration, Aghanim, N., Akrami, Y., et al. 2018, arXiv:1807.06209 [astro-ph], arXiv:1807.06209 [astro-ph]

Pujol, A., & Gaztañaga, E. 2014, Monthly Notices of the Royal Astronomical Society, 442, 1930

Pujol, A., Hoffmann, K., Jiménez, N., & Gaztañaga, E. 2017, Astronomy and Astrophysics, 598, A103

Reischke, R., Desjacques, V., & Zaroubi, S. 2019, arXiv:1909.03761 [astro-ph], arXiv:1909.03761 [astro-ph]

Rodríguez-Torres, S. A., Chuang, C.-H., Prada, F., et al. 2016, Monthly Notices of the Royal Astronomical Society, 460, 1173

Rodríguez-Torres, S. A., Comparat, J., Prada, F., et al. 2017, Monthly Notices of the Royal Astronomical Society, 468, 728

Rudd, D. H., Zentner, A. R., & Kravtsov, A. V. 2008, The Astrophysical Journal, 672, 19

Ruiz-Macias, O., Zarrouk, P., Cole, S., et al. 2020, arXiv:2007.14950 [astro-ph], arXiv:2007.14950 [astro-ph]

Saito, S., Takada, M., & Taruya, A. 2008, Physical Review Letters, 100, 191301

—. 2009, Physical Review D, 80, 083528

Sartoris, B., Biviano, A., Fedeli, C., et al. 2016, Monthly Notices of the Royal Astronomical Society, 459, 1764

Scoccimarro, R. 2015, Physical Review D, 92, arXiv:1506.02729

Scoccimarro, R., Sefusatti, E., & Zaldarriaga, M. 2004, Physical Review D, 69, 103513

Sefusatti, E., Crocce, M., Pueblas, S., & Scoccimarro, R. 2006, Physical Review D, 74, arXiv:astro-ph/0604505

Sefusatti, E., Crocce, M., Scoccimarro, R., & Couchman, H. M. P. 2016, Monthly Notices of the Royal Astronomical Society, 460, 3624

Sefusatti, E., & Komatsu, E. 2007, Physical Review D, 76, 083004

Sefusatti, E., & Scoccimarro, R. 2005, Physical Review D, 71, arXiv:astro-ph/0412626

Seljak, U. 2000, Monthly Notices of the Royal Astronomical Society, 318, 203

Sheth, R. K., & Tormen, G. 2004, Monthly Notices of the Royal Astronomical Society, 350, 1385

Skibba, R. A., van den Bosch, F. C., Yang, X., et al. 2011, Monthly Notices of the Royal Astronomical Society, 410, 417

Song, Y.-S., Taruya, A., & Oka, A. 2015, Journal of Cosmology and Astro-Particle Physics, 2015, 007

Springel, V. 2005, Monthly Notices of the Royal Astronomical Society, 364, 1105

Springel, V., Pakmor, R., Pillepich, A., et al. 2018, Monthly Notices of the Royal Astronomical Society, 475, 676

Takada, M., & Hu, W. 2013, Physical Review D, 87, 123504

Takada, M., Ellis, R. S., Chiba, M., et al. 2014, Publications of the Astronomical Society of Japan, 66, R1

Tegmark, M., Taylor, A. N., & Heavens, A. F. 1997, The Astrophysical Journal, 480, 22

Tellarini, M., Ross, A. J., Tasinato, G., & Wands, D. 2016, Journal of Cosmology and Astro-Particle Physics, 2016, 014

Tinker, J. L., Leauthaud, A., Bundy, K., et al. 2013, The Astrophysical Journal, 778, 93

Uhlemann, C., Friedrich, O., Villaescusa-Navarro, F., Banerjee, A., & Codis, S. 2020, Monthly Notices of the Royal Astronomical Society, 495, 4006

Upadhye, A., Kwan, J., Pope, A., et al. 2016, Physical Review D, 93, 063515

Vakili, M., & Hahn, C. 2019, The Astrophysical Journal, 872, 115

van Daalen, M. P., McCarthy, I. G., & Schaye, J. 2020, Monthly Notices of the Royal Astronomical Society, 491, 2424

van Daalen, M. P., Schaye, J., Booth, C. M., & Dalla Vecchia, C. 2011, Monthly Notices of the Royal Astronomical Society, 415, 3649

van den Bosch, F. C., Weinmann, S. M., Yang, X., et al. 2005, Monthly Notices of the Royal Astronomical Society, 361, 1203

Verde, L. 2010, arXiv:0911.3105 [astro-ph], 800, 147

Viel, M., Haehnelt, M. G., & Springel, V. 2010, Journal of Cosmology and Astro-Particle Physics, 06, 015

Villaescusa-Navarro, F., Banerjee, A., Dalal, N., et al. 2018, The Astrophysical Journal, 861, 53

Villaescusa-Navarro, F., Bird, S., Peña-Garay, C., & Viel, M. 2013, Journal of Cosmology and Astro-Particle Physics, 2013, 019

Villaescusa-Navarro, F., Hahn, C., Massara, E., et al. 2019, arXiv:1909.05273 [astro-ph], arXiv:1909.05273 [astro-ph]

Vogelsberger, M., Genel, S., Springel, V., et al. 2014, Monthly Notices of the Royal Astronomical Society, 444, 1518

Wadekar, D., & Scoccimarro, R. 2019, arXiv e-prints, 1910, arXiv:1910.02914

Wechsler, R. H., Zentner, A. R., Bullock, J. S., Kravtsov, A. V., & Allgood, B. 2006, The Astrophysical Journal, 652, 71

White, S. 2004, 30

Wibking, B. D., Salcedo, A. N., Weinberg, D. H., et al. 2019, Monthly Notices of the Royal Astronomical Society, 484, 989

Wolz, L., Kilbinger, M., Weller, J., & Giannantonio, T. 2012, Journal of Cosmology and Astroparticle Physics, 2012, 009

Wong, Y. Y. Y. 2008, Journal of Cosmology and Astroparticle Physics, 2008, 035

Wu, H.-Y., & Huterer, D. 2013, Monthly Notices of the Royal Astronomical Society, 434, 2556

Yamauchi, D., Yokoyama, S., & Takahashi, K. 2017, Physical Review D, 95, 063530

Yankelevich, V., & Porciani, C. 2019, Monthly Notices of the Royal Astronomical Society, 483, 2078

Yoshikawa, K., Jing, Y. P., & Börner, G. 2003, The Astrophysical Journal, 590, 654

Yoshikawa, K., Tanaka, S., Yoshida, N., & Saito, S. 2020, arXiv:2010.00248 [astro-ph], arXiv:2010.00248 [astro-ph]

Zennaro, M., Bel, J., Villaescusa-Navarro, F., et al. 2017, Monthly Notices of the Royal Astronomical Society, 466, 3244

Zentner, A. R., Hearin, A., van den Bosch, F. C., Lange, J. U., & Villarreal, A. 2016, arXiv:1606.07817 [astro-ph], arXiv:1606.07817 [astro-ph]

Zentner, A. R., Hearin, A., van den Bosch, F. C., Lange, J. U., & Villarreal, A. 2019, Monthly Notices of the Royal Astronomical Society, 485, 1196

Zhai, Z., Tinker, J. L., Becker, M. R., et al. 2019, The Astrophysical Journal, 874, 95

Zhan, H., & Knox, L. 2004, The Astrophysical Journal Letters, 616, L75

Zheng, Z., Coil, A. L., & Zehavi, I. 2007, The Astrophysical Journal, 667, 760

Zheng, Z., Berlind, A. A., Weinberg, D. H., et al. 2005, The Astrophysical Journal, 633, 791

Zu, Y., & Mandelbaum, R. 2015, Monthly Notices of the Royal Astronomical Society, 454, 1161